High Resolution Thermal Characterization and Simulation of Power AlGaN/GaN HEMTs Using Micro-Raman Thermography and 800 Picosecond Transient Thermoreflectance Imaging

Kerry Maize[1], Georges Pavlidis[2], Eric Heller[3], Luke Yates[2], Dustin Kendig[4], Samuel Graham[2], and Ali Shakouri[1]

[1]Birck Nanotechnology Center, Purdue University, West Lafayette, IN, 47907, USA, e-mail: kmaize@purdue.edu; [2]Woodruff School of Mechanical Engineering, Georgia Institute of Technology, Atlanta, GA, 30332 USA; [3]Materials and Manufacturing Directorate, Air Force Research Laboratory, Wright-Patterson Air Force Base, OH, 45433, USA; [4]Microsanj Inc., San Jose, CA, 95051, USA

***Abstract* — Self-heating in gallium nitride based high frequency, high electron mobility power transistors (GaN HEMTs) is inspected using micro-Raman thermography and 800 picosecond transient thermoreflectance imaging. The two methods provide complementary temperature information inside the semiconductor and on top metal layers of the GaN HEMT. Self heating is measured under both steady-state and ultra-fast pulsed transient operation with submicron spatial resolution, 50 milliKelvin temperature resolution, and nanosecond time resolution. Fine grain electro-thermal modeling of the HEMT steady state and transient self-heating are presented alongside measurements. Large spatial and temporal temperature gradients are quantified. Deviations due to unknown parameters are discussed.**

***Index Terms* — Gallium nitride, HEMTs, MODFETs, power transistor, Raman thermography, thermoreflectance imaging.**

I. Introduction

Gallium nitride material systems have gained attention in the power electronics community due to their high breakdown voltage and high temperature tolerance. High electron mobility transistors based on gallium nitride (AlGaN/GaN HEMTs) demonstrate robust performance under both steady state and high frequency switching operation. Despite these promising characteristics, insufficient understanding of thermal behavior and reliability has limited applicability of GaN HEMTs, especially at high power densities. Knowledge of steady state and transient temperature effects at the fail site can lead to improved designs and expanded range of application.

Multiple techniques have been proposed to measure temperature in GaN HEMTs with the required high spatial and time resolution. Raman spectroscopy has been demonstrated as a powerful technique for the quantification of temperature in AlGaN/GaN HEMTs, allowing for spatial resolution close to 0.5 μm and the identification of temperature specifically in the GaN layer or the GaN and SiC substrate simultaneously. It is possible to perform Raman in both steady state and transient modes with time resolutions on the order of 10 ns. [1]-[6] Transient thermoreflectance imaging [7]-[9], offers submicron spatial resolution and 50 milliKelvin temperature resolution. A camera acquires full field thermal images quickly with no scanning required of the measurement probe or sample. Recent enhancements using pulsed laser illumination have demonstrated transient thermoreflectance imaging with sub-nanosecond time resolution.

Combining micro-Raman and thermoreflectance imaging provides complementary measurement information particularly advantageous in thermal characterization of high frequency power semiconductor integrated electronics, such as GaN HEMTs. Raman can measure average temperature a few microns below the semiconductor surface. Thermoreflectance imaging measures temperature optimally on the device surface. Raman has been used extensively to measure temperature and stress in semiconductors whereas thermoreflectance excels at measuring temperature of metals (e.g. contacts.) By combining these techniques, it is possible to measure the transient temperature response, thermal resistances, phonon lifetimes, and thermal stresses that exist in AlGaN/GaN HEMTs with accuracy. Such parameters are necessary for the thermal analysis of these devices, providing a more complete picture of their thermal response and factors that can impact device reliability.

II. Device Description

Self-heating was studied in the high speed, gallium nitride high electron mobility transistor shown in Fig. 1. The structure consists of two 150 μm wide conducting

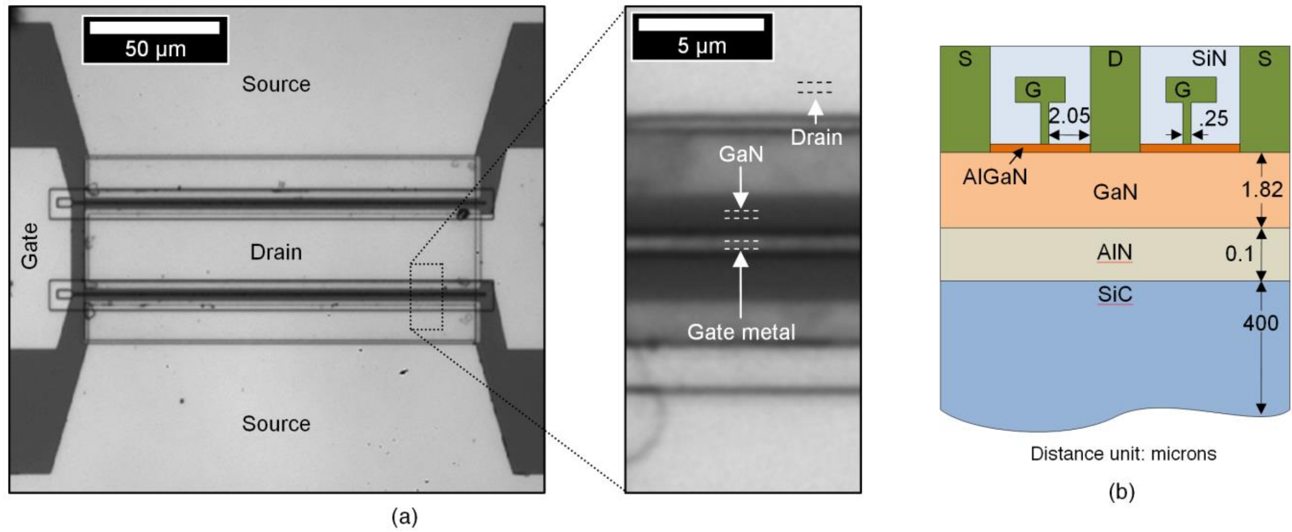

Fig. 1. (a) Optical CCD image of two finger AlGaN/GaN high electron mobility RF power transistor. Gate width ~ 150 µm. Channel length ~ 5 µm. Enlarged image shows location of thermoreflectance sampling boxes for HEMT drain metal, GaN channel, and gate metal. (b) AlGaN/GaN HEMT cross section (not to scale).

channels. Channel length of each finger is approximately 5 µm. The channels are AlGaN/GaN stacks, controlled by field effect through metal gate atop the stack. Micro-Raman and thermoreflectance measurement was performed for identical AlGaN/GaN HEMT devices. Micro-Raman spectroscopy was applied directly to the channel of the devices to measure both the average temperature rise and thermal stresses in the GaN layer. Thermoreflectance imaging analyzed temperature gradients in the HEMT gate metal, drain contact metal, and GaN channel. All Raman measurements were performed under steady state conditions while thermoreflectance was performed under pulsed operation over a range of frequencies to include both fast transient and 'quasi' steady state operating conditions.

III. Experiment Methods

A. Micro-Raman Thermography

Micro-Raman spectroscopy was performed using a Renishaw InVia Raman microscope with a 0.25 m focal length spectrometer and a 488 nm laser with a laser beam diameter 0.8 µm as the excitation source. Sub-band gap laser wavelengths were used for Raman measurements to prevent localized heating of GaN by laser light absorption. The collected Raman signals were imaged on a charge coupled device (CCD) camera. Experiments were carried out with the laser light perpendicular to the basal plane of GaN in a 180° backscattering configuration and un-polarized detection with a 50X objective. For the experiments, a 3000 l/mm grating was used with a slit width of 65 µm. An average of at least 20 measurements was made at all power conditions in order to estimate the uncertainty of the temperature measurement (95% confidence intervals).

All power sourcing and electrical measurements were conducted with a Keithley 2410 SMU for biasing the gate and a 2425 SMU for biasing the drain where high current and high voltage are needed. Ground-singal-ground probes connected to bias tees with 50 Ohm terminations were used to make electrical contact with the devices. Both the calibration and measurement steps for micro-Raman thermal metrology were done with a temperature controlled stage set at 298 K. (Instec HCP302). Thermal grease (~ 35 µm thick) was used between the backside of the wafer and the thermal stage to reduce interface thermal resistance. The resulting Raman spectrum was analyzed with a Gaussian-Lorentzian (Voigt) fit to find peak parameters of the Stokes peaks of GaN.

The temperature and the stress in the devices were estimated using the two peak fit method according to [7]:

$$\Delta\omega_{E2(High)} = A_{E2(High)}\Delta T + K_{E2(High)}\Delta\sigma \quad (1)$$

and

$$\Delta\omega_{A1(LO)} = A_{A1(LO)}\Delta T + K_{A1(LO)}\Delta\sigma. \quad (2)$$

$K_{E2(High)}$ and $K_{A1(LO)}$ are linear coefficients for the stress-phonon frequency relations, obtained by X-ray diffraction and Raman measurements on high-quality GaN templates ($K_{E2(High)}$ = -3.09 ± 0.41 cm^{-1}/GPa and $K_{A1(LO)}$ = -2.14 ± 0.28 cm^{-1}/GPa). $A_{E2(High)}$ and $A_{A1(LO)}$ describe the linear temperature-phonon frequency relations, derived by

performing Raman measurements on a high quality HVPE GaN sample subject to known temperatures from room temperature up to 673 K ($A_{E2(High)}$ = -0.0150 ± 0.0001 cm^{-1}/K and $A_{A1(LO)}$ = -0.0281 ± 0.0001 cm^{-1}/K). The residual stress was calculated using the strain-free E_2 (high) mode frequency ω_0 = 568.15 ± 0.13 cm^{-1} and the Raman biaxial conversion factor, $K_{E2(High)}$.

B. Transient Thermoreflectance Imaging

Thermoreflectance imaging microscopy measures the small change in material surface reflectance for a change in temperature. Thermoreflectance imaging of the GaN HEMT was performed by electrically probing the sample under a reflectance microscope using narrow bandwidth visible wavelength illumination. Pulsed laser illumination (440 nm) was used for 800 ps time resolution and pulsed light emitting diode illumination (530 nm) was used for 50 ns time resolution. The HEMT was electrically excited with periodic, low duty-cycle square voltage pulses at a "lock-in" signal frequency ranging between approximately one kHz to one MHz, depending on the temporal resolution desired. The voltage pulses produce self-heating in the HEMT at the lock-in frequency and corresponding reflectance change signal on the surface of the device active area. HEMT surface reflectance was recorded by an Andor 512 x 512 pixel high dynamic range electron multiplying charge coupled device camera (EMCCD) synchronized to the device lock-in excitation signal. By using pulsed illumination synchronized to the lock-in frequency, separate images of HEMT surface reflectance are recorded corresponding to the hot (on) and cold (off) time segment of the excitation cycle. Amplitude of thermoreflectance change between the hot and cold images were extracted by averaging over many HEMT excitation cycles. Thermoreflectance images with signal to noise ratios greater than five were achieved for HEMT metal regions in less than five minutes of averaging. Thermoreflectance amplitude images are converted to full field maps of temperature change across the HEMT surface by scaling with experimentally extracted material thermoreflectance coefficients, C_{TH}. Material thermoreflectance varies with wavelength of source illumination. For 530 nm LED illumination, the HEMT drain contact metal thermoreflectance coefficient was experimentally found to be $C_{TH\text{-contact metal}} = 1.6 \pm 0.23 \times 10^{-4}$ K^{-1}. Thermoreflectance coefficients for the HEMT gate metal and GaN channel were estimated indirectly based on drain contact metal coefficient using an isothermal approximation during the cooling transient for the HEMT. Estimates of thermoreflectance temperature resolution are given with each result presented in this report.

Lock-in voltage pulses during thermoreflectance imaging were applied to the HEMT drain-source with gate held constant and fully open with V_{GATE} = +2 V for all measurements. Gate leakage was negligible. Drain voltage pulse duty cycle was 15%. Pulse width and pulse amplitude are presented with results. Drain voltage pulses were supplied by a Berkeley Nucleonics voltage pulser with 3 ns rise time and 10 ns fall time. Constant gate voltage was supplied by a DC source. No bias tees were required for pulsed excitation of the HEMT. V_{DRAIN} pulse waveforms were monitored using a LeCroy high bandwidth 3.5 GHz digital oscilloscope. Current through the HEMT was measured from the pulsed voltage drop across a 50 Ω resistor in series with the HEMT drain. The HEMT was probed on wafer using Cascade Microtech ACP-40L ground-signal-ground high speed coplanar probes. Custom low profile Cascade Microtech DCQ coplanar probes were used for high magnification probing configurations. The bottom of the sample wafer was fixed by thermal paste to a two-inch thick copper heat sink maintained at room temperature.

C. Electrothermal Modeling

Transient and steady-state modeling was performed for this device using ISE Sentaurus Device [10] and based on nominal dimensions (design rules) for the device. The steady state simulation domain was about 10 μm away from the heat generating region as done in [11], with a temperature dependent thermal boundary condition linked to a large-scale 3-D finite-element thermal model built in ANSYS [12] of the device, substrate, 35 μm thermal grease (0.57 W/m/K assumed as per data sheet) and copper block held fixed at 298 K. The unusual thermal boundary in this model "A" in Fig. 2 was chosen to approximate the location of an isotherm and simplify representation of this thermal boundary layer. Model "A" is useful at very short time scales (before the heat propagates to the end of the simulation domain), and at steady state, but in between will not be accurate. A simulation "B" with a very different thermal boundary condition was used to test the region of validity of this model and disagreement of 1 K was reached at 0.3 μs. To improve this, the electro-thermal model was expanded, with an adiabatic thermal boundary condition midway between the two fingers and a 78 μm by 62 μm simulation domain containing one finger (representing twice this width and the two fingers of the actual device). Again, a simulation with a very different thermal boundary condition "C" was used to test the region of validity of this model and disagreement of 1 K was reached at 10 μs. Fig. 2 shows this process, and the level of agreement. While this complication could be eliminated with a full 3D

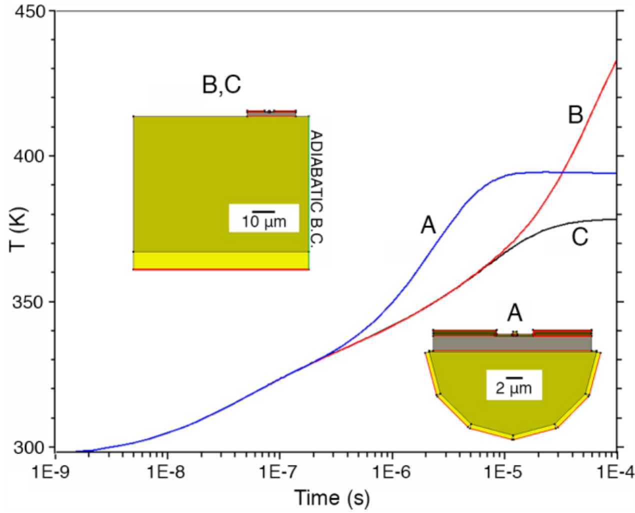

Fig. 2. Different small scale simulation domains illustrating temporal regions of validity. Drain bias is ramped up linearly over the first 1 ns of the simulation (not shown), while gate voltage was held at 0 V.

electro-thermal simulation down to the thermal sink, the process described is far more computationally efficient. In all cases, meshing was fine in regions of high gradients (electrical/thermal) such as drain corner of the gate and perpendicular to the channel and coarser away from high gradients, with verification that additional refinement did not significantly impact thermal or electrical results (~0.1%).

From this point on in the text and after Fig. 2, only simulation data in the known region of validity (prior to 0.3 µs, prior to 10 µs, or steady state depending on domain) are shown.

IV. Results

A. Results: Micro-Raman Thermography

Steady-state Raman measurements of the temperature rise between the gate and the drain are shown in Fig. 3. The data shows the maximum temperature rises 135 K above equilibrium at a power of 14 W/mm. Measurements over multiple devices on the same wafer showed repeatable results. Also, the data show a thermal resistance of 9.6 mmK/W for the devices, considering a linear power density. Fig. 4 shows the corresponding thermoelastic stress in the channel. It is shown that the induced stress is compressive and reaches a maximum near -260 MPa at a power of 14 W/mm. With a residual stress of 284 ± 18 MPa, the induced compressive stress at the highest powers reduces the average stress in the GaN layer to close to zero. However, it should be noted that inverse piezoelectric stresses has not been accounted for in this

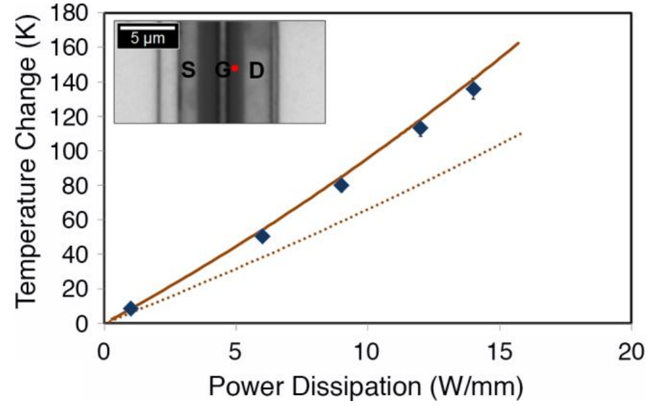

Fig. 3. Data showing the temperature rise between the gate and drain in the AlGaN/GaN HEMT under DC bias conditions, with modeled data (high thermal resistance is the solid line, lower thermal resistance is the dashed line). The laser location is represented by the red circle. A maximum temperature rise of 135 K is observed at 14 W/mm power dissipation.

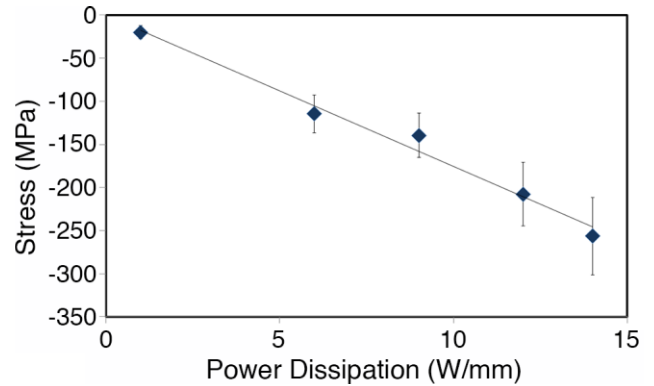

Fig. 4. Data showing the thermoelastic stress induced in the channel during DC operation. A maximum compressive stress of 260 MPa is observed at 14 W/mm power dissipation.

estimation and is expected to induce a residual tensile stress in the AlGaN layer which is still detrimental to the reliability of the device. In addition, the thermal expansion mismatch between the gate metallization and the AlGaN layer has also been shown to induce additional tensile stresses in the AlGaN region near the gate which must also be considered in the overall picture of operational induced stresses in AlGaN/GaN HEMTs.

B. Results: Transient Thermoreflectance Imaging

Pulsed illumination in thermoreflectance imaging permits capture of the time evolution of the self-heating signal within devices. The camera records reflectance data only when the light pulse is on, serving effectively as an exposure shutter to inspect selected time windows in the device excitation cycle. Temporal resolution is equivalent

to the minimum width of the light pulse. For pulsed LEDs, this is in the range of 50 ns. Transient thermoreflectance imaging using a pulsed 800 picosecond 440 nm laser has been demonstrated with subnanosecond time resolution. By controlling the delay between the phase synchronized device pulse and light pulse, individual thermoreflectance images can reconstruct the thermal transient of the device over the full excitation cycle. Fig. 5 shows the transient thermoreflectance images of the GaN HEMT using 800 picosecond pulsed illumination at 100X magnification. Images of the HEMT gate metal and drain metal thermal transient in response to a 300 ns square voltage pulse were acquired with five ns time resolution. Drain-source voltage pulse amplitude was 15 V, producing drain current of 280 mA and power of 14.3 W/mm. Fig. 5a shows the CCD image of the top HEMT channel and four false color transient thermoreflectance images of the same region at 15, 25, 50, and 100 ns after the rising edge of the excitation pulse. Images were averaged 10 minutes each. Minimum temperature resolution The plot of Fig. 5b compares the transient thermal response of the gate metal and drain metal for time = 0-50 ns. Each data point represents the mean temperature of all pixels in a sampling rectangle of width equal to the full channel width visible in the thermal image and length indicated for each region in Fig. 1a. One standard deviation for the sampled pixels was 1 K for the drain metal and 6 K for the gate metal. Ultra-fast transient thermal characterization reveal self-heating in the first 50 ns is prominent in the active channel and gate regions, indicating the occurrence of significant thermal gradients between active GaN channel and adjoining metal gate and contact regions under fast switching conditions.

The full-field view of spatial temperature distribution in the HEMT demonstrates how thermoreflectance imaging can complement micro-Raman measurement. Raman provided precise measurement of the GaN layer channel temperature at a tight spot location. Thermoreflectance imaging simultaneously provides an overview of HEMT self-heating in several adjoining regions, including the gate metal and contacts, with submicron spatial resolution.

HEMT transient self-heating was also measured beyond the first 50 ns of excitation. The full rising thermal transient from 50 ns out to ‘quasi-steady state’ at 100 µs was measured using LED based transient thermoreflectance imaging and 50X magnification. Fig. 6 plots temperature change versus logarithmic time for three critical HEMT features: GaN channel, gate metal, and drain contact. HEMT pulsed drain voltage was 20.1 V, producing drain current of 280 mA. Power was 19 W/mm. Duty cycle was 15%. The full rising transient was assembled piecewise from three separate transient imaging sweeps. HEMT temperature change within time windows one, 10, and 100 µs after the pulse rising edge were acquired using temporal resolution steps of 50 ns, 500 ns, and 5 µs respectively. One standard deviation for pixels

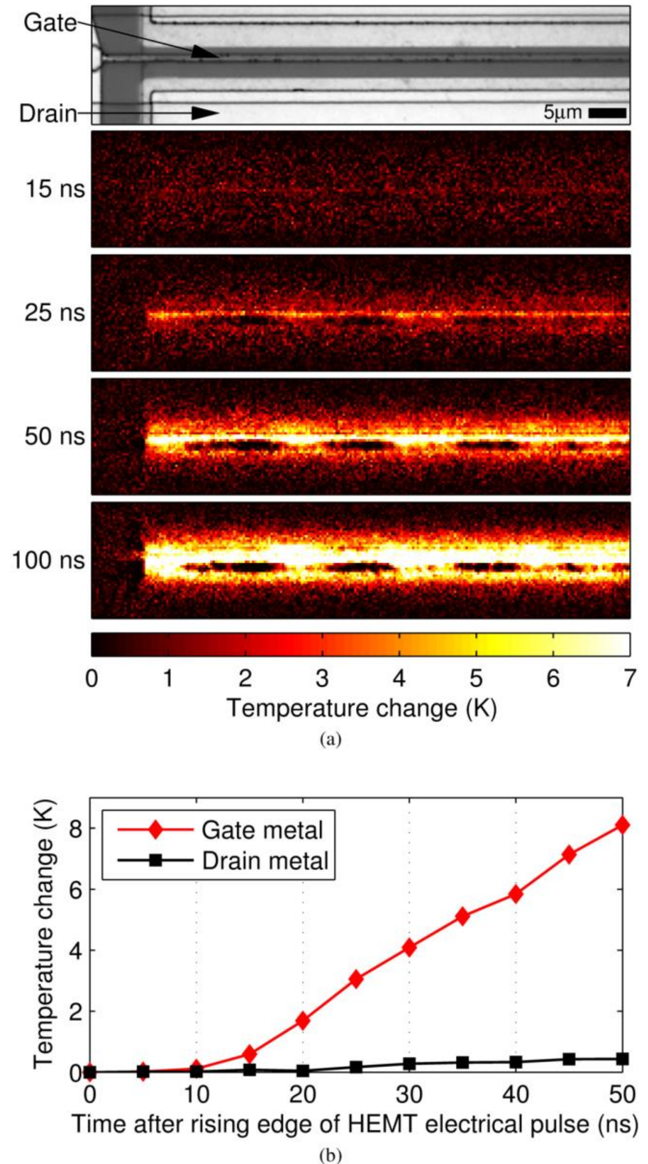

Fig. 5. Eight hundred picosecond pulsed laser transient thermoreflectance imaging of the GaN HEMT. (a) Enlarged EMCCD image of one finger in the GaN HEMT with gate metal and drain contact metal indicated. Corresponding thermoreflectance images show self-heating at 15, 25, 50, 100 ns after the rising edge of a 300 ns, 15 V excitation pulse applied to drain. (b) HEMT transient self-heating compared for the gate metal and drain metal with 5 ns time resolution. Pixel sampling region indicated in Fig. 1a. One standard deviation is 1 K for drain metal and 6 K for gate metal. Pulsed laser wavelength is 440 nm. Magnification is 50X.

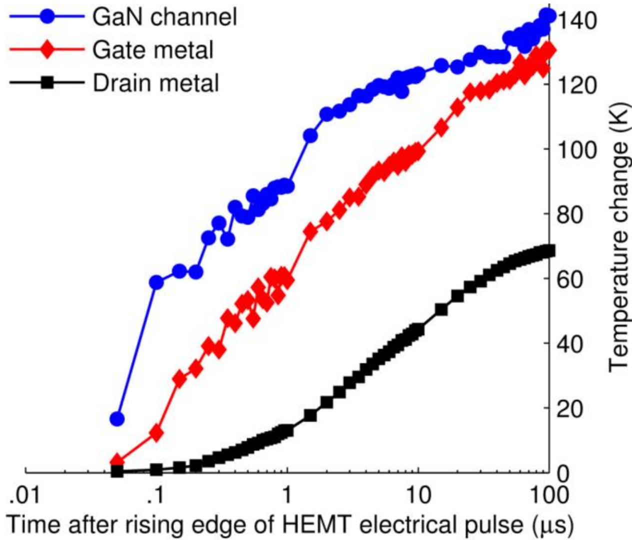

Fig. 6. AlGaN/GaN HEMT temperature rise versus logarithmic time for time = 50 ns to 100 µs after rising edge of the excitation pulse, measured with transient thermoreflectance imaging. Rising thermal transients compared for HEMT channel, gate metal, and drain contact metal regions. One standard deviation is 1, 8, and 13 K for drain metal, gate metal, and GaN channel respectively.

sampled was 1 K for the drain metal, 8 K for the gate metal, and 13 K for the GaN channel.

Comparing thermal rise times for the three HEMT features we see the GaN channel displays the fastest self-heating transient. The small gate metal heats nearly as fast as the channel. The comparatively slow thermal rise time of the drain contact metal suggests the speed at which heat from the active channel diffuses into the adjoining contacts. HEMT drain metal temperature change does not rise significantly above ~ 65 K between time = 40-100 µs, indicating the HEMT fast thermal transients have stabilized ('quasi-steady state) for pulse durations greater than 100 µs. Consequently, it is possible to estimate the HEMT thermal rise time (1-1/e) to be in the range of ~ 10 µs. The smaller and much slower 'background' thermal transients in the full chip and heat sink are expected to be on the order of 10^{-1}-10^{1} seconds.

From Fig. 6, thermoreflectance estimates GaN channel temperature rise of ~ 140 K at quasi steady state under applied bias of 19 W/mm. Using the linear thermal resistance extracted from Fig. 3, Raman measurement extrapolates GaN channel temperature rise of 182 K for the same power.

C. Results: Electrothermal Modeling

Modeling was done to compare to both the Raman and Thermoreflectance measurements, with locations of data extraction shown in Fig. 7. Because the techniques look at very different regions and time scales, data is modeled and presented differently but the same underlying model parameters were used for all models. Where simulation domain and boundary conditions were varied ("A", "B", "C"), it was verified they agree at very short times where these differences will not matter.

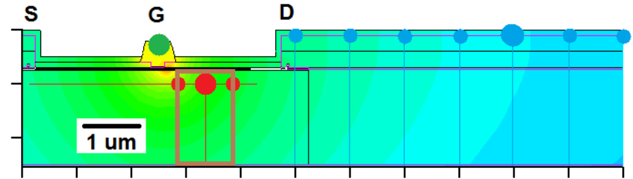

Fig. 7. Illustrates the location of data extraction, with green to represent the Thermoreflectance gate temperature measurement, the large red dot the thermoreflectance channel temperature measurement (and neighboring dots to show lateral variation), and the large blue dot the thermoreflectance ohmic temperature measurement (and again neighboring dots to show lateral variation). "S", "G", "D" show location of Source, Gate, and Drain. Last, the brown rectangle shows the location of the temperature data extraction to compare to Raman. Because the Raman laser is sub-bandgap, the data will represent an average through the thickness of the GaN and therefore model data was integrated over this region.

Fig. 8 and Fig. 9 show the modeled temperature at very short time scales, and Fig. 8 shows the transient electrical response of the modeled device. In this case, current

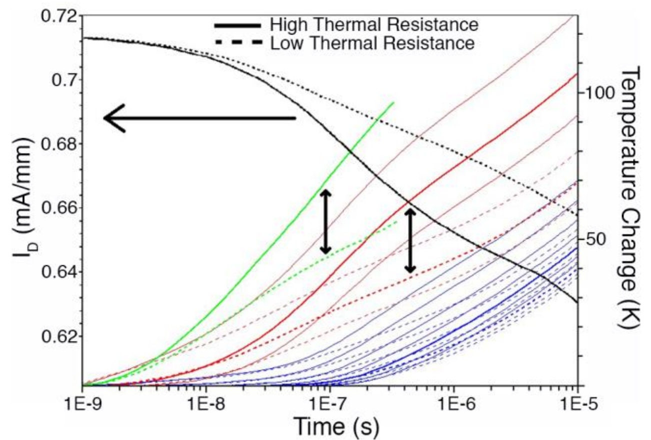

Fig. 8. Modeling results at short time scales, for the data extraction points shown in Fig. 7 (small and large red dots map to thin and thick red lines, blue to blue, green to green), and for drain current (black lines), at set bias of V_D = 20.5 V and V_G = 0 V. Because there is substantial variation for published high and low bounds to thermal resistance for the GaN epilayer and the GaN/SiC interface from ref [4], the error this can introduce in models must be understood. Double ended arrows represent the level of disagreement between modeling using optimistic or pessimistic input parameters in reported temperature at one location and effectively represent an "error bar" for modeling in the face of these unknowns.

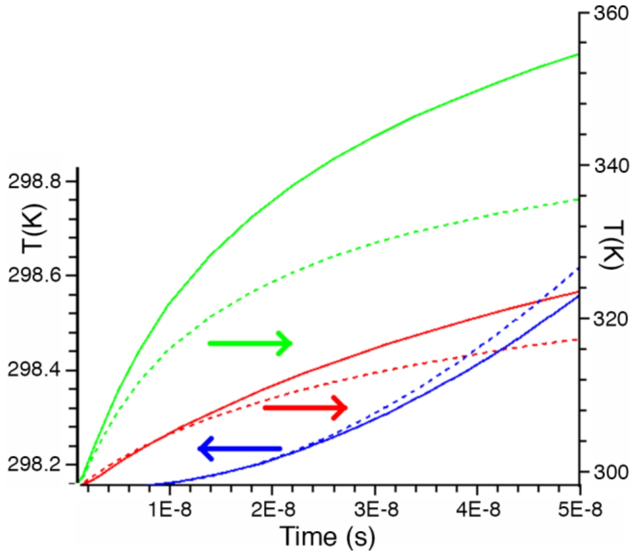

Fig. 9. Modeling results at very short time scales comparing gate, channel, and ohmic data extraction points. Zero temperature rise is at 25°C = 298.15 K at the bottom of each scale. Data extraction points are shown by the large dots in Fig. 7 (large red dots map to red lines, blue to blue, green to green). It is critical to note that the model assumed there was no thermal boundary resistance between gate and channel, so the gate heat-up in the model will be much faster than with a boundary layer in place. In fact, thermoreflectance data is seen as a way to characterize this type of unknown in the model.

droops with increasing time mostly because the electrical characteristics of the channel such as mobility and saturation velocity worsen with increasing temperature as the channel heats up. In Fig. 9, the ohmic reproduced the expected thermoreflectance data reasonably well. The gate is seen to heat up much faster than the experiment however. It is critical to note that the model assumed there was no thermal boundary resistance between gate and channel, so the gate heat-up in the model will be much faster than with a boundary layer in place. In fact, thermoreflectance data is seen as a way to characterize this type of unknown in the model.

Modeling data with respect to Raman is shown in Fig. 3 for high thermal resistance (top solid line) and low thermal resistance (bottom dotted line) at the V_D = 20.5 V and V_G = 0 V bias selected for modeling to be consistent with bias conditions and baseplate temperature selected for the Raman measurement. Other than altering AlGaN barrier thickness and composition, dimensions within the channel and epi stack, substrate mounting details and electrical properties to properly reflect the electrical properties of the devices employed in this study, the modeling methodology was entirely consistent with [1].

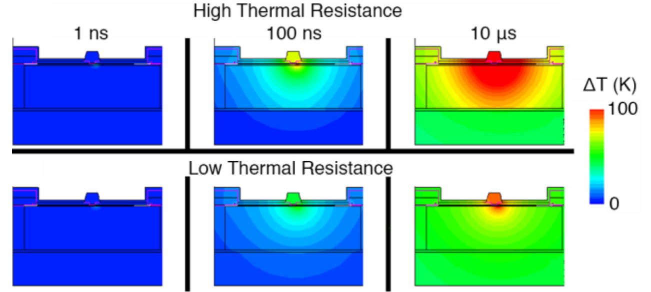

Fig. 10. Modeling results at selected times and for the high/low thermal resistance bounds. The thermal bottleneck at the GaN/SiC interface is apparent in the top row after 100 ns and 10 µs of applied power.

V. Conclusion

We have presented transient thermoreflectance imaging temperature data together with the results obtained from Raman for the GaN HEMT. Temperature gradients near the interface between the gate metal and GaN channel were inspected, as temperature related stresses here may be important in device reliability at high power density. The experimental results are compared with Sentaurus Device and finite element electrothermal modeling. From fast transient experimental and model data, we have data sufficient to begin to extract metal/semiconductor thermal interface resistances in as-fabricated devices. While the trends are consistent, some deviations are observed due to the unknown thin film thermal conductivity as well as GaN/substrate and the metal/semiconductor thermal interface resistances. As metallic layers play a key role in in-plane heat spreading, future work will use the temperature profile on the top surface at different times in order to extract key parasitic parameters and cross validate with thermal models.

References

[1] E. Heller, S. Choi, D. Dorsey, R. Vetury, and S. Graham, "Electrical and structural dependence of operating temperature of AlGaN/GaN HEMTs," *Microelectronics Reliability,* vol. 53, no. 6, pp. 872–877, 2013.

[2] R. Simms, J. Pomeroy, M. Uren, T. Martin, and M. Kuball, "Current collapse in AlGaN/GaN transistors studied using time-resolved Raman thermography." *Applied Physics Letters,* 93, 203510, 2008.

[3] A. Manoi, J. W. Pomeroy, R. Lossy, R. Pazirandeh, J. Würfl, M. J. Uren, T. Martin, and M. Kuball, "Time-dependent thermal crosstalk in multifinger AlGaN/GaN HEMTs and implications on their electrical performance," *Solid-State Electronics*, vol. 57, no. 1, pp. 14–18, March 2011.

[4] S. Choi, E. Heller, D. Dorsey, R. Vetury, and S. Graham, "Thermometry of AlGaN/GaN HEMTs using multispectral

Raman features," *IEEE Transactions on Electron Devices*, vol. 60, no. 6, pp. 1898-1904, June 2013.
[5] T. Beechem and S. Graham, "Temperature and doping dependence of phonon lifetimes and decay pathways in GaN," *Journal of Applied Physics*, vol. 103, 093507, 2008.
[6] T. Beechem, S. Graham, S. Kearney, L. Phinney, and J. Serrano, "Invited Article: Simultaneous mapping of temperature and stress in microdevices using micro-Raman spectroscopy," *Review of Scientific Instruments*, vol. 78, no.6, 2007.
[7] S. Ju, O. Kading, Y. Leung, S. Wong, & K. GooDon, "Short-timescale thermal mapping of semiconductor devices," *IEEE Electron Device Letters*, vol. 18, no. 5, pp. 169-171, May 1997.
[8] G. Tessier, S. Holé, and D. Fournier, "Quantitative thermal imaging by synchronous thermoreflectance with optimized illumination wavelengths," *Applied Physics Letters,* 78, pp. 2267-2269, 2001.
[9] M. Burzo, P. Komarov, and P. Raad, "Noncontact transient temperature mapping of active electronic devices using the thermoreflectance method," *IEEE Transactions on Components and Packaging Technologies,* vol. 28, no. 4, pp. 637-643, December 2005.
[10] Sentaurus Device User Manual, Ver. A-2007.12, Synopsys, Inc., Mountain View, CA, December. 2007.
[11] E. Heller, R. Vetury, and D. Green, "Development of a versatile physics-based finite-element model of an AlGaN/GaN HEMT capable of accommodating process and epitaxy variations and calibrated using multiple DC parameters," *IEEE Transactions on Electron Devices,* vol.58, no.4, pp.1091-1095, April 2011.
[12] ANSYS/Mechanical Software Suite, ANSYS, Inc., Canonsburg, PA.